JOURNAL OF THERMOPHYSICS AND HEAT TRANSFER
Vol. 6, No. 2, April–June 1992

Laminar Mixed Convection from a Uniform Heat Flux Horizontal Cylinder in a Crossflow

R. A. Ahmad*
Thiokol Corporation, Brigham City, Utah 84302
and
Z. H. Qureshi†
Westinghouse Savannah River Company, Aiken, South Carolina 30809

An analysis of combined forced and natural convection (mixed convection) heat transfer from a horizontal cylinder dissipating a uniform heat flux is conducted by solving the full two-dimensional steady-state Navier Stokes and energy equations. For $Pr = 0.7$, flowfields and transport results are determined in the ranges of Reynolds numbers $1 \le Re_D \le 60$ and the modified Grashof numbers $0 \le Gr_D^* \le 1.6 \times 10^4$. The results are presented as local and average values of the Nusselt number, the vorticity, the pressure distribution and the coefficient of drag around the cylinder. Correlation for the average Nusselt number and the coefficient of drag around the cylinder in the forced convection regime is suggested. Comparison with theoretical and experimental correlations is established. It was established that the Nusselt number as well as drag coefficient increase with the buoyancy parameter. It was also shown that uniform heat flux horizontal cylinder has higher Nusselt number than a cylinder under uniform surface temperature.

Nomenclature

C_D = coefficient of drag
D = diameter of cylinder, m
F = forced exerted on the cylinder, N
Gr = Grashof number based on outer radius, $g\beta(T_s - T_\infty)r_o^3/\nu^2$
Gr^* = modified Grashof number based on outer radius, $g\beta(q_s'')r_o^4/(k\nu^2)$
Gr_D = Grashof number based on outer diameter, $g\beta(T_s - T_\infty)D^3/\nu^2$
Gr_D^* = modified Grashof number based on outer diameter, $g\beta(q_s'')D^4/(k\nu^2)$
g = acceleration due to gravity, m/s²
h = local heat transfer coefficient, W/m² − K
k = thermal conductivity, W/m − K
Nu = Nusselt number based on outer radius, hr_o/k
Pe = Peclet number, $Re\ Pr$
$\tilde{P}_m$, P = dimensional (N/m²) and dimensionless pressure, respectively
P_o = normalization scale for pressure, N/m²
Pr = Prandtl number, ν/α
p^* = normalized pressure, $[P_m(\xi = 0, \eta) - P_m(\xi \to \infty, \eta)]/P_o$
q_s'' = surface heat flux, W/m²
Ra_D = Rayleigh number based on outer diameter, $Gr_D\ Pr$
Re = Reynolds number, $U_\infty r_o/\nu$
$\tilde{r}$, r = dimensional (m) and dimensionless radial coordinate, respectively
r_o = cylinder outer radius, m
T = temperature, K
U_∞ = freestream velocity, m/s
u, v = dimensionless radial and angular velocity components, m/s, respectively
$\tilde{u}$, $\tilde{v}$ = dimensional radial and angular velocity components, respectively
u_o = normalization scale for velocity, m/s
x, y = Cartesian coordinates
α = thermal diffusivity of air, m²/s
β = coefficient of volumetric expansion of air, K⁻¹
γ = angle between the forced flow direction and gravity, deg
$\Delta\xi$, $\Delta\eta$ = spacing in ξ and η directions, respectively
θ = angular coordinate, deg
κ = buoyancy parameter based on Grashof number, $Gr_D/(Re_D)^2$
κ^* = buoyancy parameter based on modified Grashof number, $Gr_D^*/(Re_D)^2$
μ = dynamic viscosity, N-s/m²
ν = kinematic viscosity, μ/ρ, m²/s
ξ, η = coordinates in the computational plane
ρ = density, kg/m³
ϕ = dimensionless temperature, $(T - T_\infty)/[(q_s'')r_o/k]$
ψ, ω = dimensionless stream function and vorticity, respectively

Subscripts
D = drag, based on diameter
F = due to friction
f = forced convection
i, j = nodal position in plane ($i = 1$ at the surface)
m = mean, due to motion
p = due to pressure
s = at the cylinder surface
τ = due to shear stress
∞ = freestream conditions

Superscripts
$-$ = average, dimensional
$''$ = flux

Presented as Paper 91-0383 at the AIAA 29th Aerospace Sciences Meeting, Reno, NV, Jan. 7–10, 1991; received Jan. 17, 1991; revision received June 3, 1991; accepted for publication June 6, 1991.

*Associate Scientist, Engineering Analysis Department. Member AIAA.
†Principal Engineer, Nuclear Engineering Section.

Introduction

Transport Mechanisms

MOST past research in the convective heat transfer area focused on either pure forced convection or pure natural convection. At high Reynolds numbers, the heat transfer occurs mainly by forced convection, but as the Reynolds number decreases, the contribution of natural convection becomes significant. Strictly speaking, in any convective heat transfer circumstance, temperature differences occur in the boundary region near the surface. These differences cause density gradients in the ambient medium, and in the presence of a body forcefield; for example, gravity, natural convection effects result. Thus, in any forced convection circumstance, natural convection effects are likely to be present.

From a practical standpoint, the question is how large these effects are, and under what conditions they may be neglected as compared to forced convection effects. On the other hand, if the buoyancy effects are of greater relative magnitude, it is the question of when forced convection effects that may be neglected. In many situations these two effects are of comparable order. Such circumstances arise from the use of hot wire/film anemometry in low velocity fields, in natural convection in the presence of ambient fluid circulations, in heat exchangers where strong temperature gradients may exist and the flow Reynolds numbers are small, and in cooling of electronic devices.

Analysis indicates the parameter that characterizes mixed convection is Gr/Re^n where Gr (Grashof number) and Re (Reynolds number) represent the vigor of a natural and forced flow, respectively. The limiting values; i.e., $Gr/Re^n \to 0$ and $Gr/Re^n \to \infty$ correspond to forced and natural convection limits, respectively. The exponent n (not necessarily equal to 2) depends on the geometry and the thermal boundary conditions. Because the distinction between the pure natural and the pure forced convection regimes is gradual, arbitrary criteria are established to identify the three transport regimes—natural, mixed, and forced convection.

The analysis of a mixed convection flow usually requires a thorough understanding of the two limiting modes. Unfortunately, mixed convection is not simply the superposition of the two modes.[1] The governing equations are coupled and nonlinear. The complexity of the transport is caused largely by interaction of buoyancy forces and a forced flowfield. If both of these effects are in the same direction, a higher transport rate in laminar flow regime will result. Surprisingly, in some turbulent flows; for example, upward forced flow in a vertical heated tube, the buoyancy forces near the wall decrease the turbulence production, resulting in reduced transport rates.[2,3] In general, for an arbitrary angle between the two forcefields, the resultant transport may be higher or even lower than that which would prevail in the presence of either effect. Additionally, the presence of buoyancy forces in a forced flow may have a significant effect on the velocity and temperature fields.

Literature Survey

Mixed convection processes may be considered in terms of external flow over surfaces, in free boundary flows (such as plumes and buoyant jets), and in terms of internal flows in tubes, channels, and enclosed flow regions. The external mixed convection flows such as over vertical surfaces, inclined and horizontal surfaces, wedges, spheres, and cylinders[4,5] have received relatively more attention because of the simplicity in analysis and in experimentation, as compared to internal flows. Details on this study are found in Refs. 4 and 5.

The problem of pure forced and pure natural convection from cylinders has been studied by many investigators.[4,5] The subsequent literature survey focuses upon mixed convection investigation from a horizontal cylinder.

As described earlier, the parameter that characterizes mixed convection is Gr/Re^n, where the value of n is between 2 and 3. Order of magnitude analysis indicates that the condition for the two effects to be of equal order is $Re_D = 0\ (Gr_D^{1/2})$.

Collis and Williams[6] in an experimental study using air recommended that the natural convection contribution in mixed convection be considered negligible when $Re > Gr^{1/3}$. Sparrow and Lee[7] obtained a solution for the mixed convection heat transfer from a horizontal cylinder for the case of aiding flow by expanding velocity and temperature profiles in powers of the distance from the lowest point on the cylinder. Joshi and Sukhatme[8] used a coordinate perturbation technique for the case of assisting and opposing free and forced convection to transform the governing equations into a system of ordinary differential equations. Merkin[9] extended the study of Sparrow and Lee[7] for large Reynolds and Grashof numbers for hot and cold cylinders using the boundary-layer equations. Jain and Lohar[10] considered the flow of a uniform stream over a horizontal circular cylinder for the case of assisting flow. Nakai and Okazaki[11] investigated the problem of mixed convection from a cylinder for the cases of parallel, cross, and contraflows. Their analysis is limited to cases where the Reynolds and Grashof numbers are very small and either forced or natural convection is dominant. Badr[12] solved the problem of combined convection heat transfer from an isothermal circular cylinder placed with its axis horizontal and perpendicular to the freestream direction. The full Navier-Stokes and energy equations were solved for the $1 \le Re_D \le 40$ and $0 \le Gr_D/(Re_D)^2 \le 5$.

Numerous papers have reported experimental results on mixed convection from a horizontal circular cylinder. Hatton et al.[13] investigated combined convection from a horizontal cylinder for the range $10^{-2} < Re_D < 45$, and Rayleigh number $10^{-3} < Ra_D\ (= Gr_D\ Pr) < 10$. The effect of freestream direction on the heat transfer process was also investigated. Oosthuizen and Madan[14] considered the problem of assisting flow in the ranges of $100 < Re_D < 3162$ and $3.75 \times 10^4 < Gr_D < 3 \times 10^5$. They suggested a correlation for the average Nusselt number. Jackson and Yen[15] have found an alternative correlation of the same data, which were found to fit the data better, especially at higher values of $Gr/(Re)^2$. In another work by Oosthuizen and Madan[16] the effect of a change in the direction of the forced flow on the heat transfer from the cylinder was investigated. No correlation was given in that

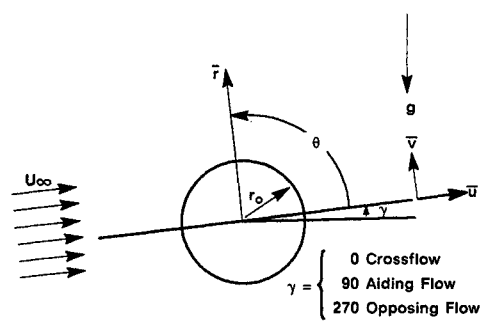

Fig. 1a Coordinate system.

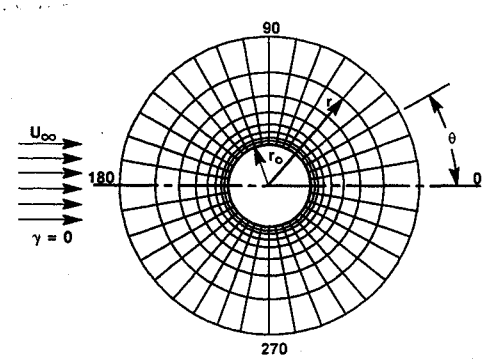

Fig. 1b Physical plane.

work. Sharma and Sukhatme[17] studied heat transfer from heated cylinders to air in crossflow. Gebhart and Pera[18] considered combined convection from very fine wires yielding small Reynolds and Grashof numbers. Nayak and Sandborn[19] made an experimental study of heat transfer from a small horizontal cylinder in an opposing forced and free convection flow. Fand and Keswani[20] studied combined natural and forced convection heat transfer from a horizontal circular cylinder to crossflow of water flowing in upward, downward, and horizontal directions. Van der Hegge Zijnen[21] made the first attempt to find a correlating equation for combined natural and forced convection effects. This procedure was to develop two equations for natural and forced convection first, then to calculate the total heat transfer as the vector sum of natural and forced heat transfer. This approach is difficult to justify on physical grounds because Nusselt numbers are not vectors.

Most of these studies consider aiding flow, in which the two effects assist each other. Few experiments and analyses have considered opposing and crossflows. For an arbitrary angle between the two effects, little work has been reported. Furthermore, almost all of the above studies consider a two-dimensional flow. The agreement between the analyses and the experiments is, in general, fairly good for vertical surfaces, whereas it is relatively poor for cylinders and spheres in mixed convection flows.

A careful review of the above mentioned literature reveals that several important aspects of mixed convection flows are still unknown. In this regard the following conclusions may be drawn:

1) There is a general lack of experimental work reporting local transport rates.

2) Boundaries between natural and mixed convection, and between mixed and forced convection are not well established for several important geometries. Furthermore, there is no general consensus about the exact form of the parameter that defines these boundaries.

Objectives and Scope of Present Investigation

The objective of the present study is to investigate mixed convection from a horizontal cylinder dissipating a uniform heat flux in air. The analysis is undertaken to cover a range of Reynolds and Grashof numbers by varying the flow velocities and surface heat flux values. The following information is specifically sought: 1) variation of local Nusselt number around the cylinder; and 2) variation of average Nusselt number with Grashof and Reynolds numbers.

Various aspects of this problem are investigated numerically. This numerical work is limited to low values of the Reynolds number. Previous studies were limited to $1 \leq Re_D \leq 40$ because steady solutions for flow around a circular cylinder become experimentally unstable with respect to asymmetric disturbances around $Re_D = 40$. The full Navier-Stokes and energy equations describing a two-dimensional mixed flow are solved. Previous studies employed boundary layer approximations that provided results for high Grashof and Reynolds numbers in the unseparated part of the boundary region. For low and moderate values of these parameters, such approximations are not always guaranteed. The numerical results provide detailed information about the velocity and thermal fields.

Analysis

Governing Equations

The steady-state, two-dimensional laminar mixed convection is governed by three conservation equations; namely, continuity, momentum, and energy. Density has been considered a variable only in formulating the buoyancy term; all other properties are taken as constant. This analysis does not consider any conduction effects within the cylinder material. The coordinate system is shown in Fig. 1a, where γ determines the angle between the forced flow direction and gravity. The dimensional constitutive equations in cylindrical coordinates are as follows:

Continuity

$$\partial\bar{u}/\partial\bar{r} + \bar{u}/\bar{r} + (1/\bar{r})\,\partial\bar{v}/\partial\theta = 0 \tag{1}$$

Momentum in Radial Direction

$$\bar{u}\partial\bar{u}/\partial\bar{r} + (\bar{v}/\bar{r})\partial\bar{u}/\partial\theta - \bar{v}^2/\bar{r} = [\rho g\beta(T - T_\infty) \cdot \sin(\theta + \gamma) - \partial\bar{P}_m/\partial\bar{r}]/\rho + \nu[\partial^2\bar{u}/\partial\bar{r}^2 + (1/\bar{r})\partial\bar{u}/\partial\bar{r} - \bar{u}/\bar{r}^2 + (1/\bar{r}^2)\partial^2\bar{u}/\partial\theta - (2/\bar{r}^2)\partial\bar{v}/\partial\theta] \tag{2}$$

Momentum in Angular Direction

$$\bar{u}\partial\bar{v}/\partial\bar{r} + (\bar{v}/\bar{r})\partial\bar{v}/\partial\theta + (\bar{u}\bar{v}/\bar{r}) = [\rho g\beta(T - T_\infty) \cdot \cos(\theta + \gamma) - (1/\bar{r})\partial\bar{P}_m/\partial\theta]/\rho + \nu[\partial^2\bar{v}/\partial\bar{r}^2 + (1/\bar{r})\partial\bar{v}/\partial\bar{r} - (\bar{v}/\bar{r}^2) + (1/\bar{r}^2)\partial^2\bar{v}/\partial\theta^2 + (2/\bar{r}^2)\partial\bar{u}/\partial\theta] \tag{3}$$

Energy

$$\bar{u}\partial T/\partial\bar{r} + (\bar{v}/\bar{r})\partial T/\partial\theta = \alpha\nabla^2 T \tag{4a}$$

where

$$\nabla^2 = [\partial^2/\partial\bar{r}^2 + (1/\bar{r})\partial/\partial\bar{r} + (1/\bar{r}^2)\partial^2/\partial\theta^2] \tag{4b}$$

Normalization

All quantities are made dimensionless by letting

$$r = \bar{r}/r_o, \quad u = \bar{u}/u_o, \quad v = \bar{v}/u_o,$$
$$\phi = (T - T_\infty)/\phi_s, \quad P = \bar{P}_m/P_o \tag{5}$$

The normalizing scales for velocity and temperature may be chosen depending upon whether the flow is dominated by forced convection or natural convection. For forced flow-dominated mixed convection, the effect of buoyancy force on forced convection is examined. Because the buoyancy force is of secondary importance, the normlization was patterned after that for pure forced convection (FC). For natural convection dominated flow, the effect of forced convection effect becomes the secondary, and the normalization was patterned after that for pure natural convection (NC). The normalizing scales used in the present analysis (Uniform Heat Flux case) are described in the following equations.

1) with normalization based on FC

$$r_o = r_o, \quad u_o = U_\infty, \quad \phi_s = (q_s'')r_o/k, \quad P_o = (1/2)\rho U_\infty^2 \tag{6a}$$

2) with normalization based on NC

$$r_o = r_o, \quad u_o = \alpha/r_o, \quad \phi_s = (q_s'')r_o/k, \quad P_o = (1/2)\rho(\alpha/r_o)^2 \tag{6b}$$

In the mixed convection regime, the converged values of the Nusselt number were matched for both normalizations.

In terms of the dimensionless variables Eq. (5), Eqs. (1–4) become:

Continuity

$$\partial u/\partial r + u/r + (1/r)\partial v/\partial\theta = 0 \tag{7}$$

Momentum in Radial Direction

$$u\partial u/\partial r + (v/r)\partial u/\partial\theta - v^2/r = (\mathrm{BB})\phi\sin(\theta+\gamma) - (1/2)\partial P/\partial r + (\mathrm{AA})[\partial^2 u/\partial r^2 + (1/r)\partial u/\partial r - u/r^2 + (1/r^2)\partial^2 u/\partial\theta^2 - (2/r^2)\partial v/\partial\theta] \quad (8)$$

Momentum in Angular Direction

$$u\partial v/\partial r + (v/r)\partial v/\partial\theta + uv/r = (\mathrm{BB})\phi\cos(\theta+\gamma) - (1/2r)\partial P/\partial\theta + (\mathrm{AA})[\partial^2 v/\partial r^2 + (1/r)\partial v/\partial r - v/r^2 + (1/r^2)\partial^2 v/\partial\theta^2 + (2/r^2)\partial u/\partial\theta] \quad (9)$$

Energy

$$u\partial\phi/\partial r + (v/r)\partial\phi/\partial\theta = (\mathrm{CC})\nabla^2\phi \quad (10)$$

where AA, BB, and CC are given as follows:
1) with normalization based on FC

$$\mathrm{AA} = 1/Re,\quad \mathrm{BB} = Gr^*/(Re)^2,\quad \mathrm{CC} = 1/Pe \quad (11a)$$

2) with normalization based on NC

$$\mathrm{AA} = Pr,\quad \mathrm{BB} = Gr^*(Pr)^2,\quad \mathrm{CC} = 1 \quad (11b)$$

Boundary Conditions

On the cylinder surface, $r = 1$:

$$u = v = 0,\quad \partial\phi/\partial r = -1 \quad (12)$$

On the far stream, $r \to \infty$: the far stream region is divided into the inflow and outflow region.

On the inflow region ($90 \le \theta \le 270$):
1) with normalization based on FC

$$u \to \cos(\theta+\gamma),\quad v \to -\sin(\theta+\gamma),\quad \phi \to 0 \quad (13a)$$

2) with normalization based on NC

$$u \to Pe\cos(\theta+\gamma),\quad v \to -Pe\sin(\theta+\gamma),\quad \phi \to 0 \quad (13b)$$

On the outflow region ($0 \le \theta \le 90$, and $270 \le \theta \le 360$):
1) with normalization based on FC

$$u \to \cos(\theta+\gamma),\quad v \to -\sin(\theta+\gamma),\quad \partial\phi/\partial r \to 0 \quad (14a)$$

2) with normalization based on NC

$$u \to Pe\cos(\theta+\gamma),\quad v \to -Pe\sin(\theta+\gamma),\quad \partial\phi/\partial r \to 0 \quad (14b)$$

Vorticity Transport Equations

The pressure term is eliminated by combining momentum and continuity equations yielding the vorticity-transport equation, which is an elliptic-type equation relating the stream function and the vorticity. The equations describing the variation of the stream function ψ, the vorticity ω, and the temperature, ϕ, are

$$\omega = \nabla^2\psi \quad (15)$$

$$u\partial\omega/\partial r + (v/r)\partial\omega/\partial\theta = (\mathrm{AA})\nabla^2\omega - (\mathrm{BB})[\cos(\theta+\gamma)\cdot\partial\phi/\partial r - (1/r)\sin(\theta+\gamma)\partial\phi/\partial\theta] \quad (16)$$

$$u\partial\phi/\partial r + (v/r)\partial\phi/\partial\theta = (\mathrm{CC})\nabla^2\phi \quad (17)$$

where

$$u = (1/r)\partial\psi/\partial\theta,\quad v = -\partial\psi/\partial r \quad (18)$$

where the dimensionless stream function and vorticity ψ and ω are related to the dimensional stream function and vorticity, $\bar{\psi}$ and $\bar{\omega}$ as
1) with normalization based on FC

$$\psi = \bar{\psi}/(U_\infty r_o) \quad \text{and} \quad \omega = \bar{\omega} r_o/U_\infty \quad (19a)$$

2) with normalization based on NC

$$\psi = \bar{\psi}/\alpha \quad \text{and} \quad \omega = \bar{\omega} r_o^2/\alpha \quad (19b)$$

The necessary boundary conditions are:
1) on the cylinder surface, $r = 1$:

$$\psi = \partial\psi/\partial r = 0,\quad \omega = \partial^2\psi/\partial r^2,\quad \partial\phi/\partial r = -1 \quad \text{and} \quad u = v = 0 \quad (20)$$

2) on the far stream $r \to \infty$: far stream region is divided into the inflow and outflow region.

On the inflow region ($90 \le \theta \le 270$):
1) with normalization based on FC

$$u \to \cos(\theta+\gamma),\quad v \to -\sin(\theta+\gamma),\quad \partial\psi/\partial r \to \sin(\theta+\gamma),\quad (1/r)\,\partial\psi/\partial\theta \to \cos(\theta+\gamma),\quad \omega = \phi = 0 \quad (21a)$$

2) with normalization based on NC

$$u \to Pe\cos(\theta+\gamma),\quad v \to -Pe\sin(\theta+\gamma),\quad \partial\psi/\partial r \to Pe\sin(\theta+\gamma),\quad (1/r)\partial\psi/\partial\theta \to Pe\cos(\theta+\gamma),\quad \omega = \phi = 0 \quad (21b)$$

On the outflow region ($0 \le \theta \le 90$, and $270 \le \theta \le 360$):
1) with normalization based on FC

$$u \to \cos(\theta+\gamma),\quad v \to -\sin(\theta+\gamma),\quad \partial\psi/\partial r \to \sin(\theta+\gamma),\quad (1/r)\partial\psi/\partial\theta \to \cos(\theta+\gamma),\quad \partial\omega/\partial r = \partial\phi/\partial r = 0 \quad (22a)$$

2) with normalization based on NC

$$u \to Pe\cos(\theta+\gamma),\quad v \to -Pe\sin(\theta+\gamma),\quad \partial\psi/\partial r \to Pe\sin(\theta+\gamma),\quad (1/r)\partial\psi/\partial\theta \to Pe\cos(\theta+\gamma),\quad \partial\omega/\partial r = \partial\phi/\partial r = 0 \quad (22b)$$

Transformation to Computational Plane

Because the stream function and vorticity vary most rapidly near the cylinder surface, a fine grid is necessary to obtain grid-independent results. To achieve this, the following transformation of the independent variables (r, θ) in the physical plane (Fig. 1b) to a new computational rectangular plane (Fig. 2) in (ξ, η) has been made by

$$r = e^{\pi\xi} \quad \text{and} \quad \theta = \pi\eta \quad (23)$$

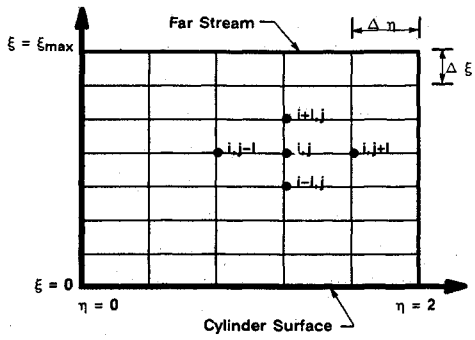

Fig. 2 Computational plane.

The Navier-Stokes and energy equations are thus transformed to

$$E^2\omega = \partial^2\psi/\partial\xi^2 + \partial^2\psi/\partial\eta^2 \tag{24}$$

$$\partial^2\omega/\partial\xi^2 + \partial^2\omega/\partial\eta^2 = (1/\mathrm{AA})[(\partial\psi/\partial\eta)(\partial\omega/\partial\xi) - (\partial\psi/\partial\xi)(\partial\omega/\partial\eta)] + E(\mathrm{BB/AA})[\cos(\pi\eta + \gamma) \cdot \partial\phi/\partial\xi - \sin(\pi\eta + \gamma)\partial\phi/\partial\eta] \tag{25}$$

$$\partial^2\phi/\partial\xi^2 + \partial^2\phi/\partial\eta^2 = (1/\mathrm{CC})[(\partial\psi/\partial\eta)(\partial\phi/\partial\xi) - (\partial\psi/\partial\xi)(\partial\phi/\partial\eta)] \tag{26}$$

where $E = \pi e^{\pi\xi}$.

The boundary conditions in the computational plane become as follows:

1) on the cylinder surface, $\xi = 0$

$$\psi = 0, \quad \omega = (1/E^2)\partial^2\psi/\partial\xi^2, \quad \partial\phi/\partial\xi = -E \tag{27}$$

2) on the far stream, $\xi \to \infty$: the far stream region is divided into the inflow and outflow region. On the inflow region ($1/2 \le \eta \le 3/2$):

1) with normalization based on FC

$$\partial\psi/\partial\xi \to E\sin(\pi\eta + \gamma), \quad \omega \to 0, \quad \phi \to 0 \tag{28a}$$

2) with normalization based on NC

$$\partial\psi/\partial\xi \to E\,Pe\sin(\pi\eta + \gamma), \quad \omega \to 0, \quad \phi \to 0 \tag{28b}$$

On the outflow region ($0 \le \eta \le 1/2$, and $3/2 \le \eta \le 2$):

1) with normalization based on FC

$$\partial\psi/\partial\xi \to E\sin(\pi\eta + \gamma), \quad \partial\omega/\partial\xi = \partial\phi/\partial\xi = 0 \tag{29a}$$

2) with normalization based on NC

$$\partial\psi/\partial\xi \to E\,Pe\sin(\pi\eta + \gamma), \quad \partial\omega/\partial\xi = \partial\phi/\partial\xi = 0 \tag{29b}$$

Finite Difference Approximations

The elliptic governing Eqs. (24) through (26) along with the boundary conditions (27) through (29) were solved by a finite difference relaxation method. The governing equations were transformed into finite difference equations by using a hybrid scheme as described by Patankar.[22] Such a scheme has been found numerically stable for convection-diffusion problems.

Figure 2 shows the coordinate system and a typical grid point i, j in the computational plane. The physical domain (Fig. 1b) was divided into a skewed (r direction) grid of size 60 × 120 grid points in the radial and angular directions, respectively. The total number of nodal points in the radial direction is fixed. Thus, the radial grid spacing is determined by the normalized distance between the cylinder surface and the outer boundary. The governing equations may now be written in their finite difference form, using the hybrid scheme. For example, the energy Eq. (26) becomes

$$\phi_{i,j}\,(\text{new}) = \phi_{i,j} + RF[(K_{i,j}\phi_{i+1,j} + L_{i,j}\phi_{i-1,j} + M_{i,j}\phi_{i,j+1} + N_{i,j}\phi_{i,j-1})/Q - \phi_{i,j}] \tag{30}$$

where RF is the relaxation factor. Its values greater than and less than unity represent over-relaxation and under-relaxation, respectively

$$Q = K_{i,j} + L_{i,j} + M_{i,j} + N_{i,j} \tag{31}$$

the coefficients in Eq. (30) are given by

$$K_{i,j} = \mathrm{MAX}[1 - (1/\mathrm{CC})(\Delta\xi/\Delta\eta)(\psi_{i,j+1} - \psi_{i,j-1})/4, \quad 0.0, \quad - (1/\mathrm{CC})(\Delta\xi/\Delta\eta)(\psi_{i,j+1} - \psi_{i,j-1})/2] \tag{32}$$

The other coefficients have similar expressions. Details on this are found in Refs. 4 and 5. The MAX represents the largest value within the brackets. The first term in the brackets represents the central difference scheme suitable for diffusion-dominated problems. Note that as the flow velocity increases the first term becomes negative. Because, for numerical stability, the coefficients in Eq. (30) must not be negative, Eq. (32) yields a value of zero for $K_{i,j}$. Thus, for the entire solution domain the coefficients in Eq. (30) remain positive or zero.

The governing equations along with the boundary conditions, in their finite difference form, were solved simultaneously by iteration. After initializing ψ, ω, and ϕ in the solution domain, the iteration sweep for the region is carried out. The solution is considered converged when the relative error between the old and the new values of ψ, ω, and ϕ becomes less than a prescribed value (typically 10^{-4}). The converged results from one run were used to initialize the other runs. The outer boundary was moved both inward and outward, keeping the number of radial grid points constant, until the heat transfer results showed no appreciable change (typically less than 1%). A typical run for a normalized distance between the cylinder surface and the outer boundary took about 700 ± 100 iterations requiring a total of about 5–8 min on an IBM 4341.

Results

The flow and temperature fields and heat transfer results were obtained for $Pr = 0.7$ in the ranges of the Reynolds numbers $1 \le Re_D \le 60$ and the modified Grashof number of $0 \le Gr_D^* \le 1.6 \times 10^4$ under crossflow conditions. It can be shown that as Reynolds number approaches zero, there is no steady-state solution for the conduction equation in cylindrical coordinates. The modified Grashof number and Rayleigh numbers were chosen because the temperature does not appear explicitly in the various transport results discussed below. In this study, the buoyancy parameter was varied between 0 and 25. Forced-flow-dominated mixed convection was analyzed in the range of $0 \le \kappa^* \le 8$, whereas natural convection dominated flow was analyzed in the range of $8 \le \kappa^* \le 25$.

Flow and Temperature Fields

Figures 3 and 4 show the streamlines and isotherms for $Re_D = 20$ and various values of the buoyancy parameter. Figure 3a shows the forced convection case where the flow divides at the forward stagnation point of the cylinder and a boundary layer builds up along the surface. The fluid accelerates when it flows past the surface of the cylinder, as can be seen by crowding of the streamlines shown and the appearance of vortex in the wake. The length of the vortex behind the cylinder is in excellent agreement with the experiment of Taneda[23]

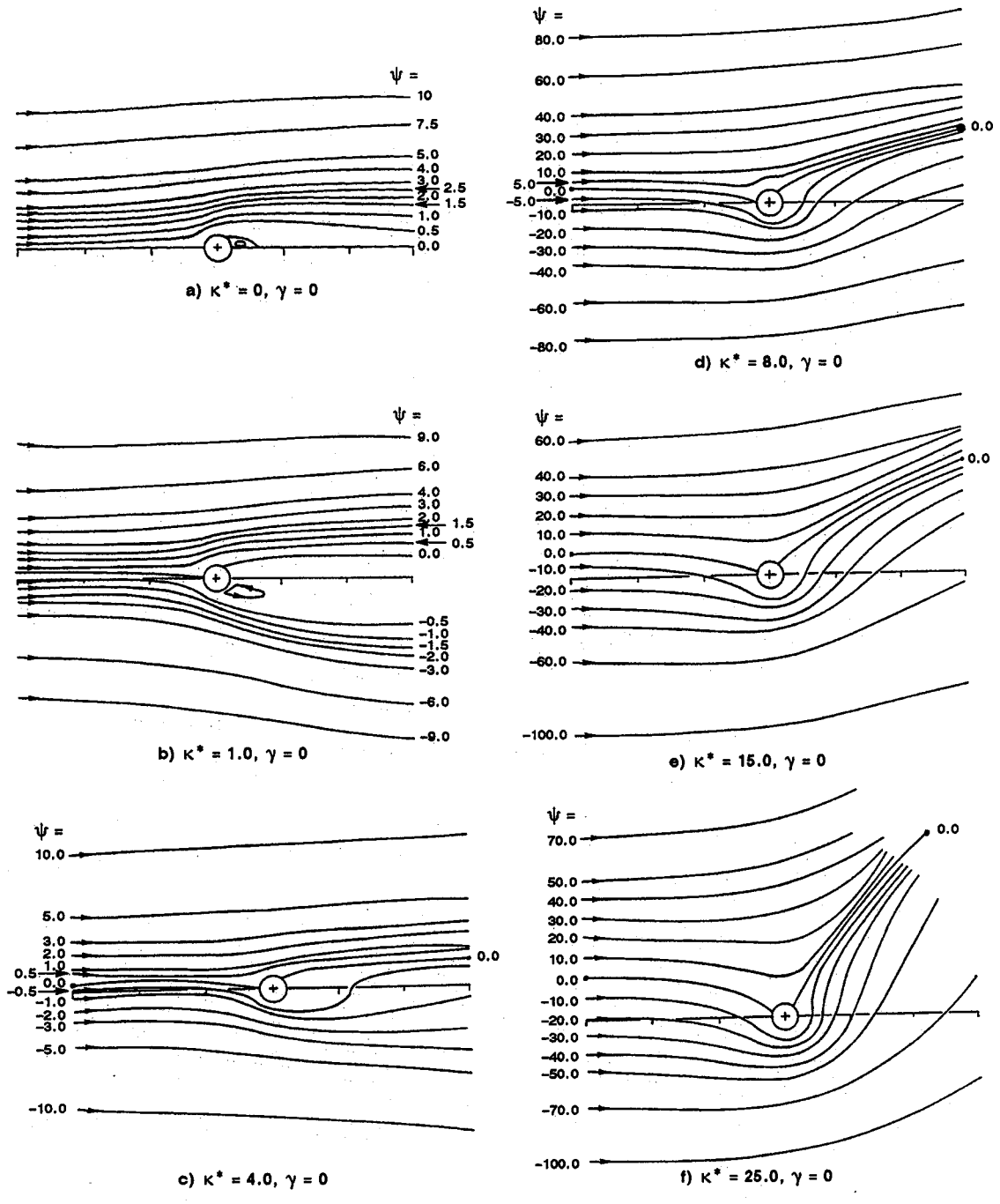

Fig. 3 Streamlines for $Re_D = 20$ and various values of κ^*; $Pr = 0.7$.

for $\kappa^* = 0$. Similarly, for the case of forced convection, the isotherms are symmetric along the direction of the flow.

The influence of the buoyancy parameter κ^* on the flow and thermal fields for the case of $Re_D = 20$ is shown in Figs. 3 and 4. As the value for the buoyancy parameter increases, streamlines ahead of the cylinder have a downward slope toward the forward stagnation point. The streamlines behind the cylinder have a positive slope and rise more in comparison to the upstream streamlines because of greater influence of the buoyancy parameter in the wake. The vortices seen for $\kappa^* = 0$ start to disappear as κ^* increases. In this study, the vortices completely disappeared for this case at $\kappa^* = 2.5$. It is believed the effect of a large buoyancy parameter on possible vortex shedding when $Re = 60$ and $0 \leq Gr_D^* \leq 1.6 \times 10^4$ would be to stabilize the flow. Results obtained by Badr[12] for an isothermal cylinder showed vortices disappeared completely for $\kappa = 1.25$ and $Re_D = 20$. Similarly, as the buoyancy parameter is increased, asymmetry in the thermal field is caused. The isotherms indicate the direction of convected heat from the cylinder and the plume formation. Results of Ref. 12 (isothermal cylinder) show that the dimensionless temperature of 0.4 at $Re_D = 20$ and $Gr_D = 2000$ ($\kappa = 5$) extended as much as 1.66 times larger than the cylinder diameter. The present results for $Re_D = 20$ and $Gr_D = 1600$ ($\kappa^* = 4$) show the dimensionless temperature of 0.4 extended as much as 1.625 times larger than the cylinder diameter. It can be deduced that the plume behind a cylinder under a uniform heat flux thermal condition may be convected to a larger distance than the same cylinder under a uniform surface temperature. This may explain the difference in the rise of the plume behind the cylinder in the present study in comparison with the results of Ref. 12. It is worth noting that isotherms emanate from the surface for the case of uniform heat flux thermal condition.

Vorticity on the Cylinder Surface

The vorticity distribution around the surface of the cylinder must be known to carry out the computation. The ω distribution is given by

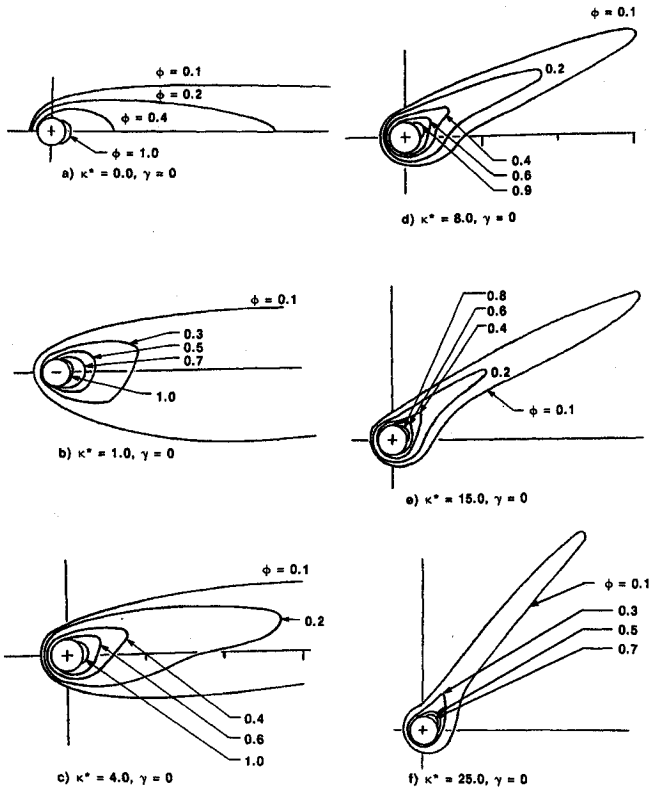

Fig. 4 Isotherms for $Re_D = 20$ and various values of κ^*; $Pr = 0.7$.

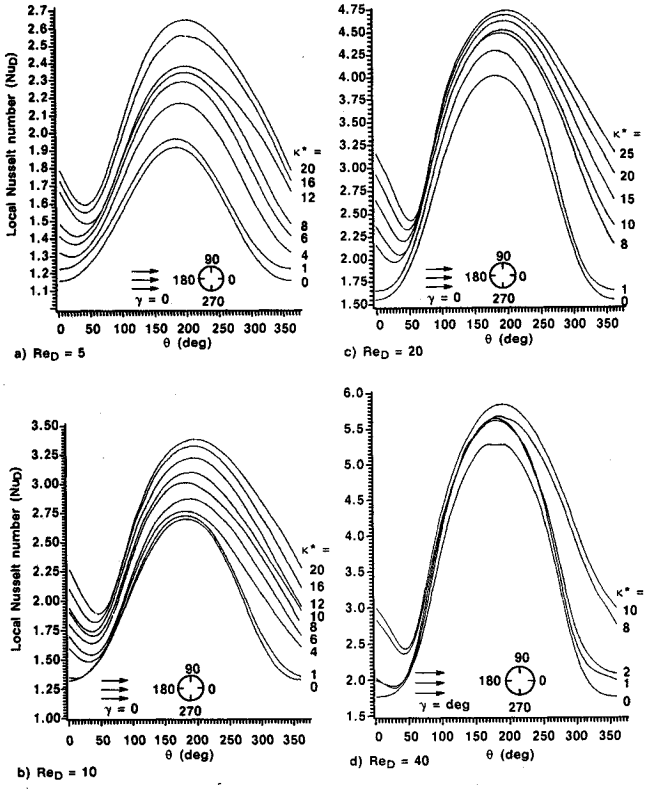

Fig. 6 Distribution of Nusselt number on the cylinder surface for $Re_D = 5$, 10, 20, and 40, and various values of κ^*; $Pr = 0.7$.

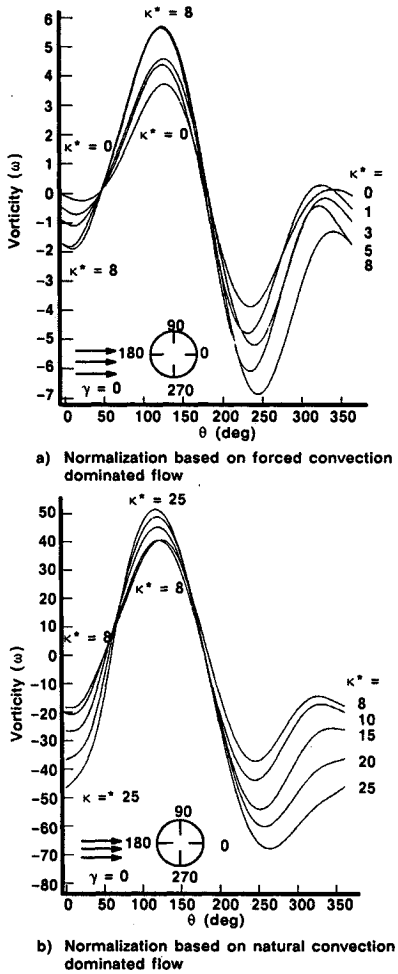

Fig. 5 Vorticity distribution on the cylinder surface for $Re_D = 20$ and various values of κ^*; $Pr = 0.7$.

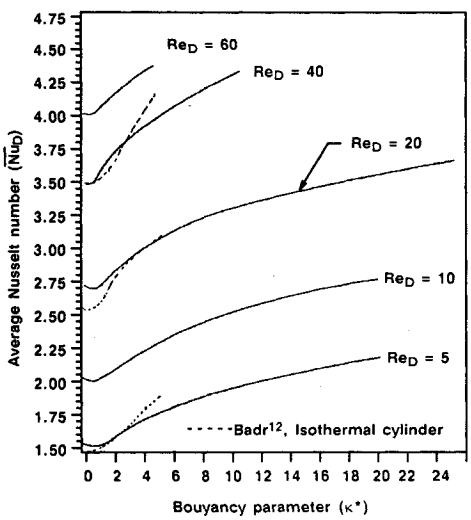

Fig. 7 Average Nusselt number vs κ^* for various values of Re_D; $Pr = 0.7$.

$$\omega_{1,j} = \left(\frac{1}{2}\right)\frac{(8\psi_{2,j} - \psi_{3,j})}{[E_s(\Delta\xi)]^2} \tag{33}$$

Figure 5 shows the variation of vorticity ω on the cylinder surface for the case when $Re_D = 20$, and for various values of buoyancy parameter κ^*. As the buoyancy parameter increases, the vorticity increases at the forward stagnation point ($\theta = 180$ deg) and reduces in the vicinity of $\theta = 250$ deg. The exact location depends on Re_D as well as Gr_D^*.

Heat Transfer

Heat transfer rates are commonly represented in terms of the local and average Nusselt numbers. The local Nusselt number is defined as

$$Nu_D(\theta) = h(\theta)D/k = \frac{(q_s'')D/k}{T_s(\theta) - T_\infty} = 2/\phi_{i,j} \tag{34}$$

The distribution of the local Nusselt number on the cylinder surface is shown in Fig. 6 for the cases of Re_D = 5, 10, 20, and 40, respectively, with different values of the buoyancy parameter κ^*. The figures show that the maximum value of Nu_D for forced convection occurs at the forward stagnation point near θ = 180 deg whereas the minimum occurs at the rear stagnation point near θ = 0. As the buoyancy parameter is increased, the maximum Nu_D continues to occur at the forward stagnation point, while the point of minimum Nu_D moves counterclockwise. The point of minimum Nu_D rises as the buoyancy parameter increases. The above expression was integrated around the cylinder to obtain the average value of the Nusselt number.

The results in Fig. 7 and Table 1 show that the buoyancy force increases the Nusselt numbers above the values that would exist in the case of pure forced convection while the Reynolds number is kept constant. It is also shown that for cases of Re_D = 5, 10, 20, and 40, the average Nusselt number decreased slightly for small values of the buoyancy parameter (κ^* = 0.5 and 0.75). This is in agreement with Hatton et al.,[13] who detected this phenomena experimentally. Based on this, neglecting the buoyancy effects for $\kappa^* < 1$ would overestimate the Nusselt number. On the other hand, at high Reynolds numbers the buoyancy effects may be negligible in comparison with forced convection.

The average Nusselt number for forced convection (κ^* = 0) results in the range of $1 \le Re_D \le 40$ was correlated as

$$\overline{Nu}_{D,f} = 0.8427(Re_D)^{0.3847} \tag{35a}$$

and the average Nusselt number for forced convection (κ = 0) results[12] (isothermal cylinder) in the range of $1 \le Re_D \le 40$ was correlated by the present authors as

$$\overline{Nu}_{D,f,UST} = 0.7860(Re_D)^{0.3968} \tag{35b}$$

where *UST* stands for uniform surface temperature. Hence, the Nusselt number obtained for the uniform heat flux boundary condition is higher than the Nusselt number obtained for the uniform surface temperature boundary condition by

$$\overline{Nu}_{D,f}/\overline{Nu}_{D,f,UST} = 1.0721/(Re_D)^{0.0121}, \quad 1 \le Re_D \le 40 \tag{35c}$$

Figure 7 shows a comparison between the results obtained from the present study for Pr = 0.7, $5 \le Re_D \le 60$, and $0 \le \kappa^* \le 25$ and the results obtained by Badr[12] for an isothermal cylinder. It can be seen that the effect of buoyancy parameter in the Badr study[12] is larger than in the present study. This is also noticed in the prediction of isotherms given in Ref. 12.

Figure 8 shows a comparison between the results obtained from the present study for Pr = 0.7, $1 \le Re_D \le 60$, Gr_D^* = 0 and nine theoretical and experimental results given in Table 2. Three of these studies were excluded because of their range of applicability. At a low Reynolds number, the present results are higher than for the isothermal cylinder case[12] and the difference decreases with the increasing of Re. This difference may be due to the surface boundary condition.

It is believed[4,5,24] that a uniform heat flux boundary condition produces a higher Nusselt number than the isothermal case. This seems to be the case even for forced convection on a flat plate. It is shown in Ref. 25 that the heat transfer coefficient for a uniform surface heat flux is 36% higher than at a comparable point on a plate with constant surface temperature.

Figure 9 shows a comparison of experimental, calculated, and theoretical studies for crossflow of air; that is, with γ = 0 deg over a horizontal cylinder. It also shows that mixed

Table 1 Drag coefficient and average Nusselt number around the cylinder surface

Re_D	Gr_D^*	κ^*	N	C_D	$\overline{Nu}_D$	Re_D	Gr_D^*	κ^*	N	C_D	$\overline{Nu}_D$
5	0	0	FC	3.74	1.52	10	0	0	FC	2.71	2.01
5	12.5	0.5	FC	3.43	1.50	10	50	0.5	FC	3.52	1.99
5	18.75	0.75	FC	4.36	1.49	—	—	—	—	—	—
5	25	1	FC	6.99	1.58	10	100	1	FC	3.40	2.04
5	50	2	FC	8.66	1.59	10	200	2	FC	4.23	2.17
5	100	4	FC	10.44	1.68	10	400	4	FC	5.29	2.21
5	150	6	FC	13.22	1.79	10	600	6	FC	7.20	2.27
5	200	8	FC	15.44	1.86	10	800	8	FC	7.77	2.44
5	200	8	NC	47.54	1.90	10	800	8	NC	90.38	2.46
5	250	10	NC	52.83	1.94	10	1000	10	NC	104.30	2.50
5	300	12	NC	59.83	2.01	10	1200	12	NC	107.05	2.59
5	400	16	NC	71.05	2.09	10	1600	16	NC	122.64	2.71
5	500	20	NC	81.04	2.19	10	2000	20	NC	146.57	2.79
20	0	0	FC	1.96	2.72	40	0	0	FC	1.24	3.52
20	400	1	FC	2.13	2.77	40	800	0.5	FC	1.18	3.43
20	1000	2.5	FC	2.29	2.89	40	1200	0.75	FC	1.13	3.62
20	1200	3	FC	2.45	2.98	40	1600	1	FC	1.30	3.72
20	1600	4	FC	2.71	3.01	40	3200	2	FC	1.47	3.79
20	2000	5	FC	2.91	3.15	40	6400	4	FC	1.56	4.02
20	2400	6	FC	2.93	3.20	40	9600	6	FC	1.68	4.05
20	3200	8	FC	3.29	3.30	40	12800	8	FC	1.87	4.23
						40	16000	10	FC	1.94	4.39
20	3200	8	NC	164.2	3.22	40	12800	8	NC	283	4.35
20	4000	10	NC	172.8	3.31						
20	6000	15	NC	202.5	3.49						
20	8000	20	NC	223.9	3.58						
20	10000	25	NC	242.6	3.72						
60	0	0	FC	0.81	4.03						
60	1800	0.5	FC	0.96	4.07						
60	3600	1	FC	1.08	4.12						
60	7200	2	FC	1.36	4.26						
60	14400	4	FC	1.89	4.39						

N = Normalization based on forced convection (FC) or natural convection (NC).

Table 2 Forced convection Nusselt number for cylinders in crossflow

					$\overline{Nu}_{Df} = a + b(Re_D)^{n1}$						
					Re_D						
	a	b	$n1$	Range of Re_D	1	5	10	20	40	60	Reference
1	0.0	0.844	0.383	1–60	0.844	1.565	2.041	2.662	3.472	4.056	Present study
2	—	—	—	1–40	0.800	1.450	—	2.540	3.480	—	Badr[12]
3	0.0	0.93	0.37	5–50	0.930	1.681	2.180	2.818	3.641	—	Eckert & Krall, from (28)
4	0.43	0.48	0.50	?–500	0.910	1.503	1.948	2.577	2.954	4.148	Hsu, from (28)
5	0.24	0.56	0.45	0.02–44	0.800	1.395	1.818	2.396	3.185	—	Collis & Williams from (28)
6	0.0	0.95	0.30	0.6–4	0.950	—	—	—	—	—	Hatton et al.,[13] from (28)
	0.0	0.81	0.38	4–40	—	1.493	1.943	2.529	3.291	—	
7	0.32	0.43	0.52	$0.1–10^3$	0.750	1.313	1.744	2.362	3.248	3.935	McAdams, from (28)
8	0.0	0.891	0.33	1–4	0.891	—	—	—	—	—	Hilpert, from (28)
	0.0	0.821	0.385	4–40	—	1.526	1.992	2.602	3.397	—	
9	0.24	0.56	0.45	0.5–12	0.800	1.395	1.818	—	—	—	Bradbury & Castro, from 28
10	0.14	0.53	0.50	10–700	—	—	1.816	2.510	3.492	4.245	Isaji & Tajima, from (28)
11	0.0	0.764	0.41	3–300	—	1.478	1.964	2.610	3.467	4.094	King, W. J., from (28)
12	0.0	0.794	0.385	0.1–50	0.794	1.475	1.927	2.516	3.286	—	Ulsamer, from (28)
13	0.0	0.795	0.384	1–35	0.795	1.475	1.925	2.512	—	—	Morgan[28]
	0.0	0.583	0.471	35–5000	—	—	—	—	3.313	4.010	

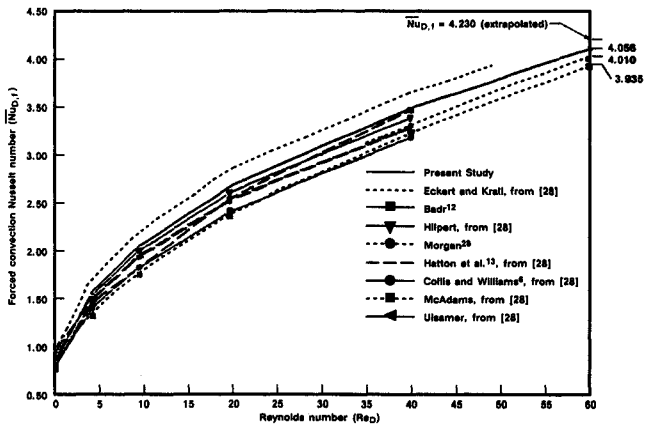

Fig. 8 Comparison between the forced convection Nusselt number from the present study and previous experimental and theoretical results.

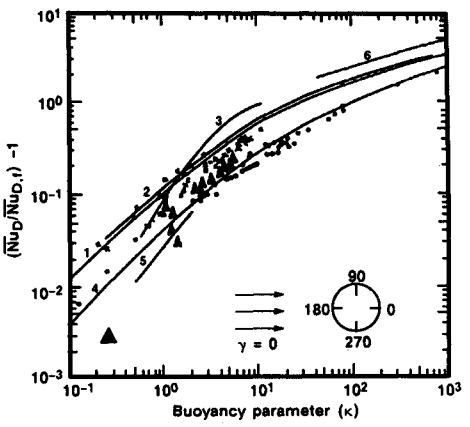

1 Eq (41), Ref. 28
2 Data of Sharma and Sukhutme[17], isothermal
3 Data of Oosthuizen and Madan[16], isothermal
4 Eq (41), water, Ref. 28
5 Fand and Keswani's[20], Eq (17) (zone 2), water
6 Fand and Keswani's[20], Eq (25) (zone 4), water
• Laminar boundary layer, data of Fand and Keswani[20], water
o Separated boundary layer, data of Fand and Keswani[20], water
▲ Badr[12], isothermal cylinder
x Present study, uniform heat flux case

Fig. 9 Comparison between experimental and calculated Nusselt numbers for mixed convection around a cylinder in crossflow of air.

convection heat transfer is higher from experiments than for theoretical studies. This is to be expected because the theoretical study[12] and the present study considered laminar mixed convection. Purely laminar conditions are difficult to achieve experimentally. It also shows the Nusselt number from an isothermal cylinder[12] is lower than the Nusselt number from the same cylinder under a uniform heat flux boundary condition (present study) in a laminar mixed convection regime.

Pressure Distribution on Cylinder Surface

Once the distribution of ω and ϕ are known, the pressure variation around the surface of the cylinder is given by

$$P^*(\xi = 0, \eta) = [P_m(\xi = 0, \eta) - P_m(\xi \to \infty, \eta)]/P_o$$

$$= c_3 \int_0^{\eta_j} (\partial\omega/\partial\xi)_{1,j}\, d\eta_j'$$

$$+ c_4 \int_0^{\eta_j} \phi_{i,j}\cos(\pi\eta_j' + \gamma)\, d\eta_j' \qquad (36a)$$

where c_3, c_4 and P_o are given as follows:

1) with normalization based on FC

$$c_3 = -2/Re, \quad c_4 = 2\pi Gr^*/(Re)^2, \quad P_o = (1/2)\rho U_\infty^2 \qquad (36b)$$

2) with normalization based on NC

$$c_3 = -2Pr, \quad c_4 = 2\pi Gr^*(Pr)^2, \quad P_o = (1/2)\rho(\alpha/r_o)^2 \qquad (36c)$$

The subscript $1,j$ refers to any angular position on the cylinder surface. Figure 10a indicates the direction of the pressure force on the surface of the cylinder. Let $F_{p,x}$ and $F_{p,y}$ be the pressure forces per unit length exerted in the x and y directions, respectively, and F_τ to be the shear force per unit length. Therefore

$$F_{p,x} = -\iint \bar{P}_m\cos(\theta + \gamma)\, dA$$

$$= -r_o \int_0^{2\pi} \bar{P}_m\cos(\theta + \gamma)\, d\theta \qquad (37)$$

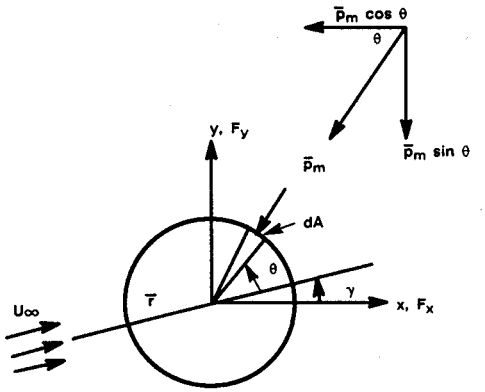

Fig. 10a Pressure force on a circular cylinder.

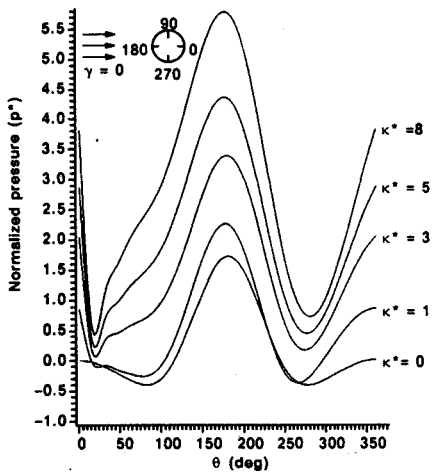

Fig. 10b Pressure distribution on the cylinder surface for $Re_D = 20$ and various values of κ^*; $Pr = 0.7$. (Normalization based on forced convection dominated flow.)

$$F_{p,y} = -\iint \bar{P}_m \sin(\theta + \gamma)\, dA$$

$$= -r_o \int_0^{2\pi} \bar{P}_m \sin(\theta + \gamma)\, d\theta \tag{38}$$

and

$$F_\tau = -\iint \tau_{r\theta} \sin(\theta + \gamma)\, dA$$

$$= -r_o \int_0^{2\pi} \tau_{r\theta|r=r_o} \sin(\theta + \gamma)\, d\theta \tag{39}$$

The pressure distribution around the cylinder for the case of $Re_D = 20$ is shown in Fig. 10b for various values of the buoyancy parameter κ^*. The forced convection case ($\kappa^* = 0$) is shown in each figure for comparison reasons. It can be seen that the pressure at the rear stagnation point $\theta = 0$ is zero. This is consistent with the Kirschoff-Helmholtz[26] solution, where the pressure is zero everywhere inside the wake. It is also consistent with Kawaguti and Jain.[27]

These figures also show that as Gr_D^* increases, pressure is also increased around the cylinder. The maximum value of pressure continues to occur at the forward stagnation point while the point of minimum pressure moves counterclockwise. The point of minimum pressure rises as the buoyancy parameter increases. This is to be expected because the rise of the rear streamlines are indicative of the rise of the wake.

The normalized pressure increased as a result of the presence of the buoyancy force, above that which would exist for a purely forced convection case at the same Reynolds number.

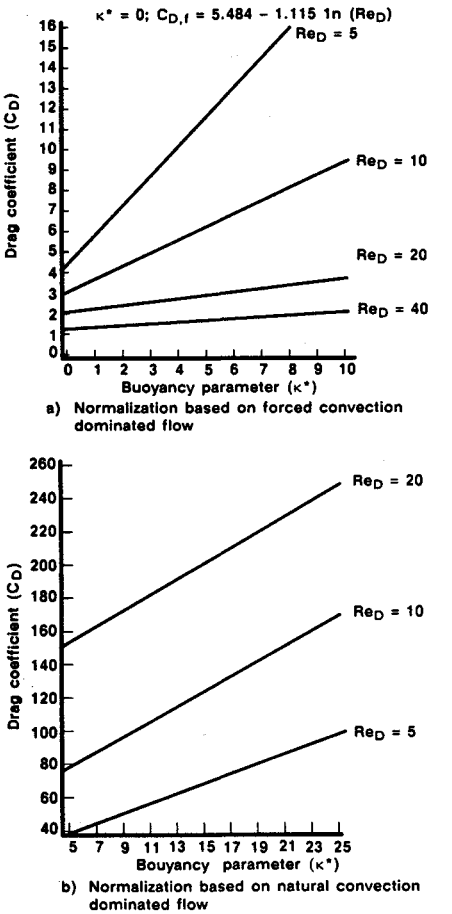

Fig. 11 Drag coefficient vs κ^* for various values of Re_D; $Pr = 0.7$.

Drag Coefficient

The coefficient of drag due to pressure forces can be divided into two components.

1) with normalization based on FC, we get

$$C_{D,p} = -(\pi/2)\left[\int_0^2 P_{1,j}\cos(\pi\eta_j + \gamma)\, d\eta + \int_0^2 P_{1,j}\sin(\pi\eta_j + \gamma)\, d\eta\right] \tag{40a}$$

The frictional contribution to the drag coefficient is calculated by

$$C_{D,F} = (\pi/Re)\int_0^2 \omega|_{\xi=0}\sin(\pi\eta_j + \gamma)\, d\eta \tag{40b}$$

2) With normalization based on NC, we get

$$C_{D,p} = -(\pi/2)\left[\int_0^2 P_{1,j}\cos(\pi\eta_j + \gamma)\, d\eta + \int_0^2 P_{1,j}\sin(\pi\eta_j + \gamma)\, d\eta\right] \tag{41a}$$

$$C_{D,F} = +(\pi Pr)\int_0^2 \omega|_{\xi=0}\sin(\pi\eta_j + \gamma)\, d\eta \tag{41b}$$

The total coefficient of drag is calculated as

$$C_D = C_{D,p} + C_{D,F} \tag{42}$$

The drag coefficient results given in Fig. 11 show the same behavior as the heat transfer results. The drag coefficient increased as a result of the presence of the buoyancy force, above that which would exist for a purely forced convection case at the same Reynolds number. The coefficient of drag for forced convection $\kappa^* = 0$ results in the range of $1 \leq Re_D \leq 40$ was correlated as

$$C_{Df} = 5.484 - 1.115 \ln (Re_D) \quad (43)$$

Conclusions

The following statements summarize the conclusions that were reached.

1) It was found that a uniform heat flux cylinder (present study) has higher Nusselt number than the same cylinder under uniform surface temperature boundary condition.

2) The correlated Nusselt number in the forced convection regime from the present study is compared with other correlations found in literature. The agreement is quite good.

3) Heat transfer and drag coefficients in the mixed convection regime increased considerably above the values that would exist in purely forced convection.

4) The flow and thermal fields have been found to be affected by the buoyancy parameter κ^*.

5) The direction of forced flow on natural convection drastically affects the transport rates from the surface.

Acknowledgment

This study was supported by the National Science Foundation under grant MEA-8204361 and the University of Illinois Research Board. The computer time at the University of Illinois Computer Center is appreciated.

References

[1]Acrivos, A., "Combined Laminar Free and Forced Convection Heat Transfer in External Flows," *AIChE Journal,* Vol. 4, No. 3, 1958, pp. 285–289.

[2]Axcell, B. P., and Hall, W., "Mixed Convection to Air in a Vertical Pipe," *Proceedings of the Sixth International Heat Transfer Conference,* Hemisphere Publishing Corporation, Toronto, Vol. 1, 1978, pp. 37–42.

[3]Connor, M. A., and Carr, A. D., "Heat Transfer in Vertical Tubes Under Conditions of Mixed Free and Forced Convection," *Proceedings of the Sixth International Heat Transfer Conference,* Hemisphere Publishing Corporation, Toronto, Vol. 1, 1978, pp. 43–48.

[4]Ahmad, R. A., "Mixed Convection Around a Horizontal Cylinder," Ph.D. Thesis, Univ. of Illinois, Chicago, 1985.

[5]Ahmad, R. A., and Qureshi, Z. H., "Laminar Mixed Convection from a Uniform Heat Flux Horizontal Cylinder in a Crossflow," AIAA Twenty-ninth Aerospace Sciences Meeting and Exhibit, AIAA Paper 91-0383, Jan. 1991.

[6]Collis, D. C., and Williams, M. J., "Two-dimensional Convection From Heated Wires at Low Reynolds Number," *Journal of Fluid Mechanics,* Vol. 6, 1959, pp. 357–384.

[7]Sparrow, E. M., and Lee, L., "Analysis of Mixed Convection About a Horizontal Cylinder," *International Journal of Heat and Mass Transfer,* Vol. 19, 1976, pp. 229–232.

[8]Joshi, N. D., and Sukhatme, S. P., "An Analysis of Combined Free and Forced Convection Heat Transfer From a Horizontal Circular Cylinder," *Journal of Heat Transfer,* Vol. 93, 1971, pp. 441–448.

[9]Merkin, J. H., "Mixed Convection From a Horizontal Circular Cylinder," *International Journal of Heat and Mass Transfer,* Vol. 20, 1977, pp. 73–77.

[10]Jain, P. C., and Lohar, B. L., "Unsteady Mixed Convection Heat Transfer From a Horizontal Circular Cylinder," *Journal of Heat Transfer,* Vol. 101, 1979, pp. 126–131.

[11]Nakai, S., and Okazaki, T., "Heat Transfer From a Horizontal Circular Wire at Small Reynolds and Grashof Number—II," *International Journal of Heat Mass Transfer,* Vol. 19, 1976, pp. 229–252.

[12]Badr, H. M., "A Theoretical Study of Laminar Mixed Convection From a Horizontal Cylinder in Cross Stream," *International Journal of Heat Mass Transfer,* Vol. 26, 1983, pp. 639–653.

[13]Hatton, A. P., James, D. D., and Swire, H. W., "Combined Forced and Natural Convection with Low-speed Air Flow Over Horizontal Cylinders," *Journal of Fluid Mechanics,* Vol. 42, 1970, pp. 17–31.

[14]Oosthuizen, P. H., and Madan, S., "Combined Convective Heat Transfer From Horizontal Cylinders in Air," *Journal of Heat Transfer,* Vol. 92, 1970, pp. 194–196.

[15]Jackson, T. W., and Yen, H. H., "Combined Forced and Free Convection Equations to Represent Combined Heat Transfer Coefficients For Horizontal Cylinders," *Journal of Heat Transfer,* Vol. 93, 1971, pp. 247–248.

[16]Oosthuizen, P. H., and Madan, S., "The Effect of Flow Direction on Combined Convection Heat Transfer from Cylinders to Air," *Journal of Heat Transfer,* Vol. 93, 1971, pp. 240–242.

[17]Sharma, G. K., and Sukhatme, S. P., "Combined Free and Forced Convection Heat Transfer From a Heated Tube to a Traverse Air Stream," *Journal of Heat Transfer,* Vol. 91, 1969, pp. 457–459.

[18]Gebhart, B., and Pera, L., "Mixed Convection From Long Horizontal Cylinders," *Journal of Fluid Mechanics,* Vol. 45, 1970, pp. 49–64.

[19]Nayak, S. K., and Sandborn, V. A., "Periodic Heat Transfer in Directly Opposed Free and Forced Convection Flow," *International Journal of Heat and Mass Transfer,* Vol. 20, 1977, pp. 189–194.

[20]Fand, R. M., and Keswani, K. K., "Combined Natural and Forced Convection Heat Transfer from Horizontal Cylinders to Water," *International Journal of Heat and Mass Transfer,* Vol. 16, 1973, pp. 1175–1191.

[21]Van Der Hegge Zijnen, B. G., "Modified Correlation Formulae For Heat Transfers by Natural and Forced Convection From Horizontal Cylinders," *Applied Scientific Research,* Vol. A6, 1956, pp. 129–140.

[22]Patankar, S. V., *Numerical Heat Transfer of Fluid Flow,* McGraw-Hill, New York, 1980.

[23]Van Dyke, M., *An Album of Fluid Motion,* Parabolic Press, Stanford, CA., Chap. 2, 1982.

[24]Qureshi, Z. H., and Ahmad, R. A., "Natural Convection From A Horizontal Cylinder at Moderate Rayleigh Numbers," *Numerical Heat Transfer,* Vol. 11, 1987, pp. 199–212.

[25]Kays, W. M., and Crawford, M. E., *Convective Heat and Mass Transfer,* McGraw-Hill, 1980, Chap. 9, 2nd ed.

[26]Fornberg, B., "A Numerical Study of Steady Viscous Flow Past a Circular Cylinder," *Journal of Fluid Mechanics,* Vol. 98, 1980, pp. 819–855.

[27]Kawaguti, M., and Jain, P., "Numerical Study of a Viscous Fluid Flow Past a Circular Cylinder," *Journal of the Physical Society of Japan,* Vol. 21, 1966, pp. 2055–2062.

[28]Morgan, V. T., "The Overall Convective Heat Transfer from Smooth Circular Cylinder," *Advances in Heat Transfer,* Vol. 11, 1975, pp. 199–264.